Fabrication and Functionalization of 3D Printed Polydimethylsiloxane-Based Microfluidic Devices Obtained through Digital Light Processing

Fabrication and Functionalization of 3D Printed Polydimethylsiloxane-Based Microfluidic Devices Obtained through Digital Light Processing

*Gustavo Gonzalez, Annalisa Chiappone, Kurt Dietliker, Candido Fabrizio Pirri, Ignazio Roppolo**

G. Gonzalez, Dr. A. Chiappone, Prof. C. F. Piri, Dr. I. Roppolo

Dipartimento di Scienza Applicata e Tecnologia, Politecnico di Torino, C.so Duca degli Abruzzi 24, 10129, Turin, Italy

PolitoBIOMed Lab, Politecnico di Torino, C.so Duca degli Abruzzi 24, 10129, Turin, Italy

E-mail: ignazio.roppolo@polito.it

G. Gonzalez, Prof. C. F. Pirri

Center for Sustainable Futures @Polito, Istituto Italiano di Tecnologia, Via Livorno 60, 10144, Turin, Italy.

Prof. Kurt Dietliker

Department of Chemistry and Applied Biosciences, ETH Zurich, Vladimir-Prelog-Weg 1, 8093 Zurich, Switzerland.

Abstract

This work reports the preparation and 3D printing of a custom-made photopolymer based on acrylate-polydimethylsiloxane (PDMS), for the fabrication of complex-shaped 3D printed microfluidic chips. By selecting and combining the proper materials during the preparation of the resins along with the freedom of design of light-based 3D printers, 3D microfluidic PDMS-like chips were obtained with excellent optical features, high chemical stability, and good mechanical properties. Furthermore, taking advantage of unreacted functional groups exposed on the sample's surface after the 3D printing step, the surface properties of the devices were easily and selectively modified during the post-curing step through UV-induced grafting polymerization techniques, giving an added value to the printed devices in terms of surface treatment compared to conventional methods. The 3D printing of the PDMS-based resins developed here may potentially transform the fabrication methodology of PDMS microfluidic devices by decreasing manufacturing costs and time, allowing the production of complex-shaped and truly three-dimensional microdevices.

Keywords:

3D printing; microfluidics; photopolymerization; silicone materials; surface functionalization

1. Introduction

Over recent years, microfluidic systems have attracted attention in the scientific and industrial community, particularly in the medical and pharmaceutical fields. They have the potential to perform accurate laboratory analysis on a much smaller scale compared to current procedures, leading to reduced sample consumption, costs, and instrument size. [1,2] A typical microfluidic device is a set of micro-scale channels fabricated for handling small quantities of fluids to perform precise chemical and biological analyses. [3–5] These devices could be used for different applications, for instance, rapid DNA sequencing and electrophoretic separation [6,7] or for disease diagnosis in point-of-care settings with a high level of precision. [8,9] However, one of the crucial points in the development of a

microfluidic device is the correct choice of the material for the fabrication. [10,11] One of the most commonly used materials in microfluidics is polydimethylsiloxane (PDMS) polymer. [12] This elastomeric material offers valuable properties especially for biological applications, such as biocompatibility, transparency, water and gas permeability, mechanical resistance, besides being an inexpensive polymer. [13–15]

PDMS-based microfluidic devices are usually fabricated through Soft Lithography, a high-precision technique that involves a substantial level of human labor and high investment costs, which make the diffusion of these devices beyond research laboratories difficult. Furthermore, Soft-Lithography only allows the manufacture of two-dimensional PDMS devices. [2] Therefore, to expand the capabilities of microfluidic devices towards new horizons, it is essential to develop new methods that allow their production in shorter times, at lower costs and maintaining good precision.

Recently, polymeric three-dimensional printing (3DP) technology has emerged as a promising alternative to Soft-Lithography for the fabrication of microfluidic devices, [16–19] and is becoming one of the most outstanding technologies today. [20,21] Interest in 3D printing has been increasing in the last few years due to the multiple and attractive features involved in this technology, considered one of the fundamental pillars of the industry 4.0. [22–24] 3D printing technology has been used in applications such as robotic, aerospace, bioelectronic and medicine among others. [25–29] This technology involves a series of processes and techniques in which digital designs are used to build up a component by depositing materials layer by layer. [30,31] Through this manufacturing technique, truly three-dimensional, complex-shaped and bespoke microfluidic devices can be fabricated in a single step within minutes or hours, replacing expensive manual microfabrication methods and simplifying the manufacture of complex lab-on-chip (LOCs) devices concerning conventional fabrication systems such as Soft-Lithography. [32] In this manner, microfluidic chips could become more accessible to researchers and industrial users in different applications fields, leading to accelerated innovation in the microfluidic world.

The most widely used 3D printing techniques for the fabrication of polymeric microfluidic devices include fused filament fabrication (FFF), Inkjet/Polyjet, and stereolithography (SLA) or digital light processing (DLP) [18]. The last two techniques, based on spatially controlled solidification of photosensitive liquid resins, are known to be the most versatile methods [30] since they combine high printing resolution with affordable prices in materials and equipment. Furthermore, they allow the production of objects with particular properties just by fine-tuning the main ingredients of the photocurable formulation. [33] A typical liquid resin for light-based 3D printing is made of three main ingredients: (i) the oligomer/monomer, which determines the final physical and mechanical characteristic of the printed structure, (ii) the photoinitiator, which establishes the reactivity of the resin for the light-induced polymerization reaction and (iii) a dye or colorant which controls the light penetration during 3D printing (*Z-axis*) and ensures a high resolution (*XY plane*).

Taking this into consideration, some researchers have achieved 3D printed polymeric structures with specific properties or functionalities by tailoring the main elements of the printable liquid formulation [33–35] or by adding functional additives. [36–40] For instance, Stassi et al. developed 3D printed microcantilevers (MCs) for mass-biosensing by adjusting the content of acrylic acid monomers in the printable formulation, obtaining structures with different amounts of available active carboxylic groups on the surface [33], whilst Li et al. obtained 3D printed dental objects with fascinating antibacterial properties by loading quaternary ammonium salts as antimicrobial agents in a thiol-ene-acrylate resin. [40] Recently, using poly(dimethylsiloxane)-based photopolymers, well-defined three-dimensional objects were obtained via thiol-ene crosslinking chemistry through a customized top-down 3D printer [41], while in a pioneering work, Folch and coworkers used methacrylate PDMS formulations to produce optically transparent structures and microfluidic channels using a commercial desktop-SL 3D printer. [42]

In this work we aim at making a further step forward in the fabrication of microfluidic devices with PDMS-like features: first, we show the preparation and 3D printing of a photocurable formulation based on acrylate polydimethylsiloxane (PDMS) for the realization complex-shaped 3D printed

microfluidic devices employing a commercial 3D-DLP printing. The 3D printed PDMS-like samples are compared to classical PDMS polymers commonly used in the fabrication of microfluidic chips through Soft-Lithography. Furthermore, taking advantage of unreacted acrylic double-bonds after the 3D printing step, we exploited the usual UV post-curing step to attach functional molecules (carboxylic groups) on the surface of the microchannels, through a UV-induced grafting polymerization technique. Thereby we selectively functionalize the samples' surface, allowing to widen the range of 3D printed silicones in terms of surface properties, especially if compared to classical PDMS materials. A series of assessments were performed to optimize the preparation of the printable formulation, followed by chemical and mechanical characterizations of the produced silicone samples. The 3D printing of PDMS-like devices may potentially transform the traditional fabrication of PDMS-based microfluidic devices by decreasing manufacturing costs and time, allowing the production of complex-shaped and truly three-dimensional microdevices.

2. Results and discussion

2.1 Photopolymerization characterization and 3D printing

To achieve the target properties and find optimized parameters for the 3D printing step, preliminary studies were performed for the preparation of the silicone-based photopolymer. One of the most challenging issues for silicone oligomers is that they are highly hydrophobic, [43,44] which can make difficult the dispersion of photoinitiators and dyes; this is problematic as they are essential elements for the preparation of a suitable 3D printable formulation. The TRAD liquid oligomer used here has low compatibility with many chemicals, and become hazy almost instantaneously when mixed with other materials. Thus, special efforts were made for the correct preparation of the TRAD-based formulation to obtain a printable resin with good optical properties. The first criterion was to select an appropriate photoinitiator. It is important that the photoinitiator is soluble in the acrylic-PDMS oligomer and absorbs in the wavelength of the desktop 3D printer, which is 405 nm. Under these

conditions, the most frequently used photoinitiators for 3D printing applications are phosphine oxide-based compounds (TPO and BAPO). [45–47] These photoinitiators have been reported in the literature for silicone-based formulations,[41,42,48] however they do not mix well in the TRAD oligomer. Therefore, we selected a phosphine-oxide derivate photoinitiator specifically synthesized for this approach (BAPO-Si, Figure SI 1). [49] This photoinitiator is a yellowish liquid type I photoinitiator, with an absorption spectrum (Figure SI 2) and a photoactivity similar to the commercially available phenyl bis(2 4 6-trimethylbenzoyl)phosphine oxide (BAPO). Nevertheless, we noticed that when adding more than 0.6 wt.% to the TRAD oligomer, the formulation lost its transparency. Consequently, downstream experiments were made by fixing 0.6 wt.% of BAPO-Si as optimum photoinitiator concentration.

A light absorber (or dye) is commonly added to the formulation at low concentration to obtain well-defined 3D printed objects. [50] The addition of a light-absorbing in the formulation helps to control the spatial parameters (resolution) during printing, by limiting the propagation of the photopolymerization reaction both on the *Z*-direction and on the *X*-*Y* plane. The second criterion was therefore to choose an appropriate dye. The dye chosen was a disperse red 1- based molecule bearing a methacrylate group (DR1-MA) (Figure SI 1.c). This commercial dye was selected because due to its methacrylate functionality, it can co-polymerize during the photopolymerization process in the 3D printing step, and remain covalently linked to the polymer network after the polymerization process. This strategy of integrating the dye in the polymer backbone avoids the uncontrolled and long-term release of dye during the use of the microfluidic device. This solves one of the main problems of 3D printed microfluidic devices, namely the contamination of the fluids passing through the microfluidic channels. [51] However, since DR1-MA is not directly mixable in acrylate-polydimethylsiloxane we used a small amount of methyl methacrylate (MMA) to disperse the dye. [45]

Preliminary tests for the printability of the silicone-based formulation with DLP-type 3D printers were performed through real-time photo-rheology methods. In **Figure 1**.a, the storage (G') and loss (G'') moduli are plotted versus irradiation time for a TRAD formulation loaded with 0.6 wt. % of

BAPO-Si photoinitiator and 0.1 wt.% of DR1-MA dye. Initially, the storage modulus (G') is lower than the loss modulus (G''), indicating the liquid-like viscous behavior of the pre-polymer before the light illumination. Once the lamp is turned on and the photopolymerization is triggered, the G' curve becomes predominant and crosses the G'' curve, reflecting the elastic response of the material with a solid-like behavior. The crossover of the two curves (G'=G'') is the gelation point of the formulation, which is reached after about 9.1 seconds of visible light illumination (Figure 1.a).

The reactivity of the silicone-based resin was evaluated with the ATR-FTIR technique in order to minimize the effect of oxygen inibition in radical photopolymeryzation. The spectra were recorded for both liquid formulations and solid samples at different fabrication stages, as described in the Experimental section.

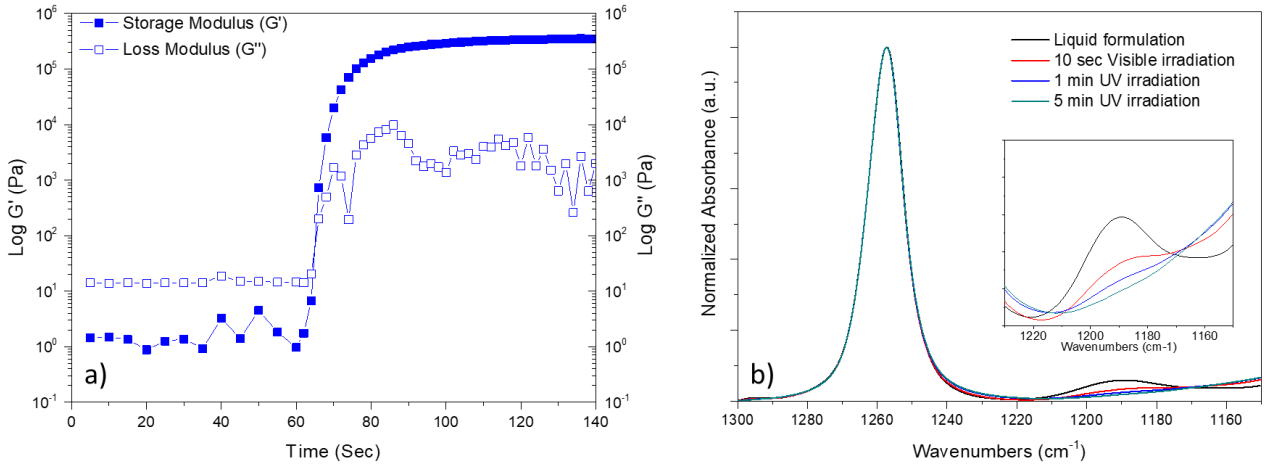

Figure 1. a) Storage modulus (G') and loss modulus (G'') against illumination times and b) ATR-FTIR spectra TRAD samples after different times of irradiation (full spectra in figure SI 3) showing in the inset the magnification of the acrylate double bond decrease in the range 1220-1170 cm^{-1}.

Figure 1.b shows the decrease of the 1196 cm^{-1} peak, after different irradiation times, associated with the single carbon-oxygen bond of acrylate moieties whose vibrations are altered by the reaction of acrylate bonds after polymerization. [52] The areas underneath the peaks were normalized using as a reference the signal centered at 1257 cm^{-1}, which correspond to methyl siloxane stretching vibrations. [53] The ATR-FTIR results at different stages of the process are reported in Figure SI 3, while the most important data for 3D printing process are summarized in Table 1. Following 10 seconds of visible

light exposure, the formulation reached 74 % of acrylate conversion. This conversion is acceptable in view that the irradiation was performed under a standard environmental atmosphere, where oxygen-induced inhibition prevents complete conversion due to the well-known phenomenon of radical scavenging. Although 74 % is not particularly high, it is, however, adequate to build the piece during 3D printing; indeed, for this stage, it is enough that the piece reaches the gelation point [54] as shown during the photorheology experiments. The acrylate conversion further increases after 1 and 5 minutes of post-curing UV irradiation, to 97 % and 98 %, respectively.

Table 1. Acrylate conversion (%) for TRAD formulation after visible light irradiation (10 seconds), 3D printing with similar irradiation conditions followed by 5 minutes of UV post-curing irradiation and some mechanical properties of the 3D printed TRAD samples compared to those values for classical PDMS Sylgard 184 taken from literature. TRAD formulation contained 0.6 wt.% of BAPO-Si and 0.1 wt.% of DR1-MA.

Sample condition	Acrylate conversion (%)		Young's modulus (MPa)	Ultimate tensile stress (MPa)	Elongation at break (%)
	Real-time irradiation[a)]	3D printed			
Photopolymerized	74	78	1.4 ±0,1	0.66 ± 0.13	63 ± 20
5 min UV post-curing[b]	98	94	1.5 ± 0.1	0.70 ± 0.11	62 ± 15
PDMS Sylgard 184 (10:1) at 25 °C [15]	-	-	1.32 ± 0.07	5.13 ± 0.55	93.1

[a)] Measured through ATR-FTIR after direct irradiation of visible (10 sec) and UV light (5 min).
[b)] Evolution of acrylate conversions after different UV irradiation time is shown in Figure SI 4.

Once the formulation was optimized, the following step was to print different types of 3D objects to demonstrate the suitability of our novel silicone-based resin in the fabrication of complex structures and microfluidic chips. Figure 2.a shows the photographs of microfluidic chips with an S-shaped channel of 800 µm of diameter, filled with a green-colored water solution. Figure 2.b shows a 3D printed chip consisting of two wells (with dimensions analogous to a single well of 96-multiwell plate used for cell culture) connected by a 1x1 mm^2 microfluidic channel with a transparent bottom of 500 µm (see Figure 2.d). More complex-shaped 3D printed structures were also obtained as shown in Figure 2.c, which reports a trapezoidal chip in which inside it hosts a three-dimensional channel with a square section of 1x1 mm^2 (see Figure SI 11.c for more details). The printed elastomer exhibited

excellent stretchability as shown in Figure 2.e for a 3DP strip wrapped in a cylinder of 3 mm of diameter. The 3DP structures were scrubbed with compressed air to remove the excess of resin in the channels before the post-curing step; they were then rinsed in ethanol for 15 min and dried at room temperature overnight. The just-printed parts presented an adequate acrylate conversion of 78 % as observed in Table 1, and after 5 minutes of UV post-curing, the maximum acrylic conversion was measured to be 94 % (Figure SI 3.c-d and Figure S4).

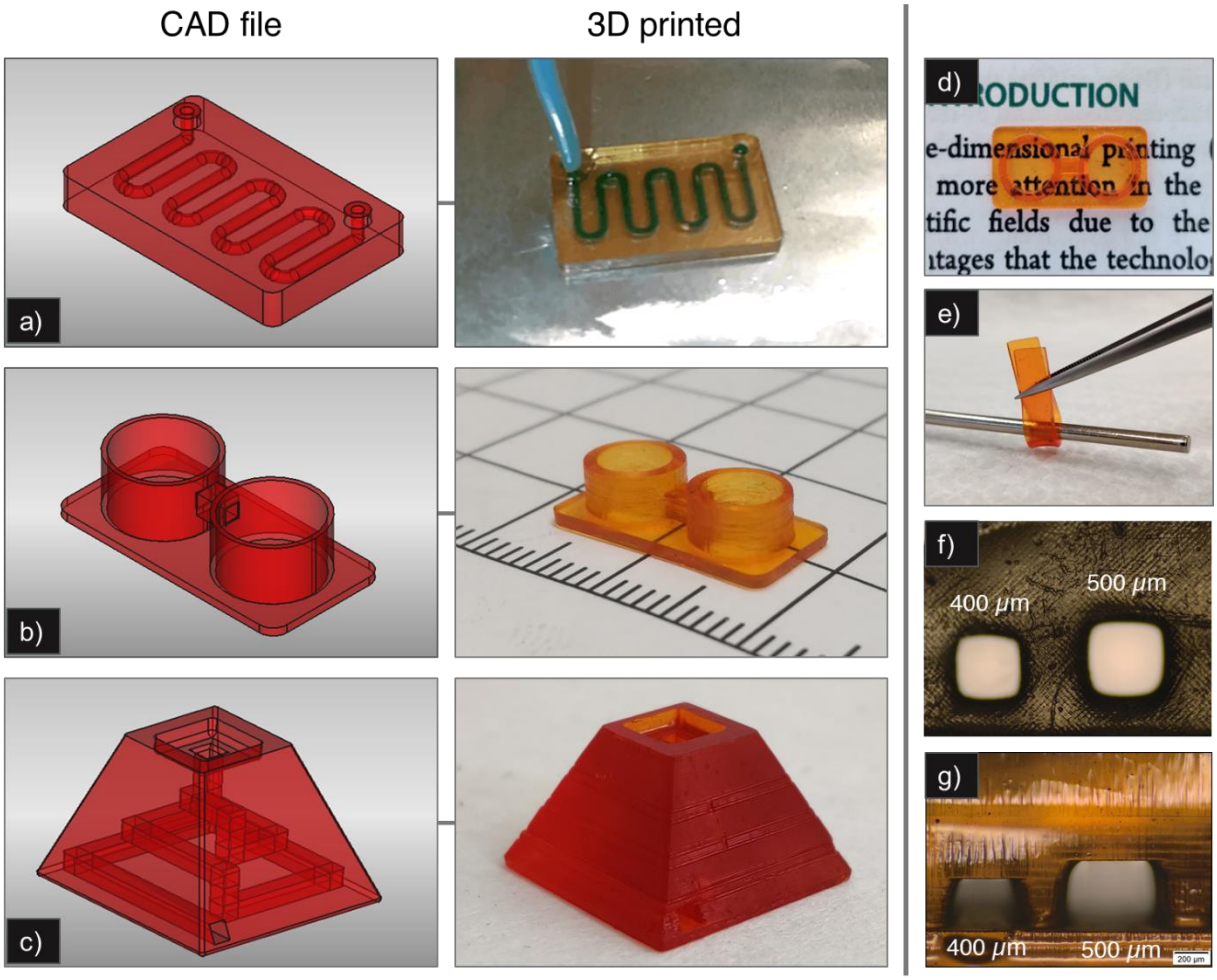

Figure 2. CAD design illustration and photographs of different microfluidic chips. a) 3D printed microfluidic chip with an s-shaped channel of 800 µm of diameter, where the channel is filled with green colored water, b) two 3D printed wells connected by a 1x1 mm^2 square section channel, c) trapezoidal 3D printed microfluidic chip with a 1x1 mm^2 channel square section, d) photograph of the two 3D printed 96-wells showing the transparency of the bottom with 500 µm thickness, e) a 3D printed strip (20x5x1 mm3), showing the excellent stretchability of the material when wrapped around a 3 mm diameter cylinder. Photograph (10x) of the smallest microchannel achieved in f) XY-plane and g) Z-axe.

Regarding the printing resolution, the smallest channel achieved was 400x400 μm^2 both in the *X*-*Y* plane and in the Z-axis, as shown in Figure 2.f and 2.g, respectively. Smaller features (< 400 µm) were not obtained due to the problematic removal of uncured resin, which remained trapped in the

channel and caused clogging. However, these results are in good agreement with the current literature, slightly improving the smallest microchannel dimensions for 3D printed PDMS-like materials (500x500 μm^2) found elsewhere. [42] Moreover, a truly 3D microchannel architecture was obtained, which can be exploited for different applications such as for the manufacturing of complex and passive microfluidic mixer with various 3D configurations [55] or the fabrication of a three-dimensional lab-on-a-chip for cell culture and biological analysis. [56]

2.2 Solvent stability of the 3D printed material

After the 3D printing step and the post-curing process, not all the components of the formulation (oligomer, monomers, photoinitiators and light absorber) end up in the photo crosslinked. These residual elements might be detrimental since in microfluidic devices the unreacted materials could diffuse through the liquid passing into the channels of the chip during operations, potentially contaminating the fluids. Therefore, it is important to develop a more thorough cleaning protocol to remove or extract all uncured residual elements from 3D printed parts. For this purpose, dissolution extension of the 3DP TRAD samples towards different solvents was measured by determining the swelling weight percent (wt.%) following a 24-hour immersion in a variety of solvents and the extracted weight percent (wt.%) of uncured resin from dried samples. Results are summarized in Table 2 and plotted in Figure SI 5.c. 3DP TRAD samples swelled significantly more in non-polar and in some polar-aprotic solvents, such as DCM (229.7 %), THF (204.4 %), cyclohexane (184.5 %) and toluene (169.2 %), followed by acetone (27,1 %) and isopropanol (17.9 %). Regarding the extraction of uncured resins, the higher the capacity of a solvent to penetrate the matrix, the higher the efficiency of extraction; this occurred for DCM, THF, cyclohexane, toluene, and acetone. However, once removed from the respective solvent after 24-hours of immersion, all the samples were damaged on the surface, except for the one immersed in acetone. This was attributed to the inability of the polymer to sustain the stresses generated on the surface during the uneven evaporation of these highly swelling solvents, which produced irreversible defects.

Table 2. Swelling percentage (wt.%) of 3D printed TRAD samples after immersion for 24 hours and 1 hour, as well as extracted resin percentage (wt.%) of samples after 24 hours of immersion in different solvents at 25°C.

Chemical	Swelling (wt.%) *after 24-h immersion*	Extracted resin weight (wt. %)	Swelling (wt.%) *after 60-min immersion*
Isopropanol	17.9	7.0	14.4
Acetone	27.1	7.5	25.8
Ethanol	5.1	5.0	4.5
Distilled Water	1.4	1.8	1.3
Hydrogen Peroxide	1.7	2.6	1.6
Acetonitrile	6.4	0.7	6.3
Dimethylformamide (DMF)	8.7	2.6	7.7
Dimethyl sulfoxide (DMSO)	9.8	2.6	5.2
Cyclohexane	184.5	9.2	161.8
Tetrahydrofuran (THF)	204.4	10.8	180.2
Dichloromethane (DCM)	229.7	12.5	192.5
Toluene	169.2	8.7	168.4

Another important point is that most of the microfluidic devices usually operate for relatively short times during their usage (i.e. a fluid is passing through the microchannel). Therefore, it is important to know the stability of the 3D printed TRAD parts (post-cured, washed and dried samples) towards different solvents for brief periods. The dimensional stability of 3DP samples was determined by performing swelling tests for short intervals of 5, 10, 15, 30 and 60 minutes; the results are plotted in Figure SI 5.a-b and summarized in Table 2 (only for 60 minutes of immersion). As discussed, 3DP TRAD samples present different swelling percentage behaviors according to the solvent used. [57] After 60 minutes of immersion, the lowest values obtained were in distilled water (1.3%), while the highest values were reached using DCM (plateau reached at 30 min) and THF. This information is useful when envisaging how to employ these devices in different microfluidic applications.

Out next approach was aimed at selecting the appropriate solvent for a washing protocol that completely removes all unreacted elements within the samples without deteriorating or damaging the 3D structures. Based on previous results, acetone was selected as the washing solvent, since it offers the best compromise between efficient extraction of residual material and no significant deterioration of the samples. Therefore, a series of washing procedures were performed using acetone, and ultraviolet-visible spectra of the washing solvent were collected (see Figure SI 6). With short washing times, all the other curves showed a shoulder around 300 nm corresponding to the absorbance of

unreacted BAPO-Si (see Figure SI 2) photoinitiator, while after 5 hours of washing treatment the analyzed solvent did not present any trace of residual substances. Equally important, there was no release of the DR1-MA dye at each washing time, thus confirming the copolymerization of the dye into the polymer backbone during the photopolymerization process. [58]

2.3 Mechanical tests

The mechanical properties of the 3DP TRAD samples were also determined and compared to the properties of conventional PDMS polymers (Figure SI 7). Tensile test specimens were 3D printed (dog bone with a gauge length of 20 mm), and each sample was exposed to a post-curing treatment under UV irradiation for 5 minutes on each side. Then the specimens were washed and dried following the protocol developed here for the TRAD microfluidic devices: immersion in acetone for 6 hours (using fresh solvent every hour) and overnight drying treatment at 120 °C. Besides, only 3D printed samples with no UV post-curing treatment were also tested for comparison reasons. The samples were mechanically tested to obtain ultimate tensile stress, fracture stress, and elongation at break. Tensile results are summarized in Table 1 and plotted in Figure SI 8 for UV post-cured and just 3D printed samples, both containing 0.6 wt.% of BAPO-Si photoinitiator and 0.1 wt.% of DR1-MA dye.

Young's modulus and ultimate tensile stress (UTS) values were slightly higher in UV post-cured samples than in 3D printed samples with no UV treatment, while elongation at break values are similar for both classes of samples. Appreciable differences were observed when comparing tensile results of the 3DP TRAD samples with those for conventional 10:1 PDMS (Sylgard 184). While Young's Modulus was similar, UTS values were considerably lower for 3D printed samples. Moreover, even elongation at break was lower in 3D printed samples. This could be attributed to the fact that in 3D printing processes layer defects are randomly generated: they act as nucleation points for cracks initiation and decrease the material's strength.

2.4 UV-induced surface modification

The surface functionalization of PDMS microfluidic chips is an essential goal to increase the versatility of these devices towards both well-established and new applications. There is a vast literature on methods for surface functionalization of microfluidic channels, which includes photo-mediated graft polymerization of monomers such as PEGDMA, pNIPAAm or acrylic acid onto PDMS [59–61] as well as more elaborate methods based on "click" chemistry for the grafting of alkyne-PEG [62] or thiol groups. [63] Although these methods show an outstanding surface modification capability, they require a multiple-step procedure to achieve the functionalization of the samples.

Taking advantage of the characteristics of the 3DP TRAD samples, here we introduce an easy and selective surface functionalization method. Once the 3D printing step was completed, the printed parts still have unreacted functional acrylic groups, as previously demonstrated by FT-IR analyses. For this reason, a post-UV-curing treatment is usually performed on the samples to reach the maximum acrylic conversion, leading to improve, for example, the mechanical properties of the part. [64] The unreacted acrylic double-bonds in our 3D printed parts can be exploited to attach other functional molecules through UV-induced "grafting to" polymerization techniques. [65] Considering this, we took advantage of the required UV post-curing treatment to contemporaneously achieve the highest possible acrylic conversion and functionalize the polymer surface. Initially, 3D printed flat samples (10x15x1.5mm, *lwh*) were used for surface modification experiments. The grafting solution consisted of acrylic acid (AA) diluted in acetonitrile (100 mg mL^{-1}) and 2 wt.% (concerning the AA amount) of phenyl bis(2,4,6-trimethylbenzoyl) phosphine oxide to activate the polymerization. The procedure for the UV-induced surface modification is sketched in Figure 3.a. A few drops of the grafting solution were spread on the sample, then it was irradiated with ultraviolet light for different times (1, 5 and 10 min), with 10 mW cm^{-2} of light intensity. Afterward, the samples were rinsed with ethanol for 10 min and washed extensively with deionized water for 30 minutes to remove unlinked polyacrylic acid.

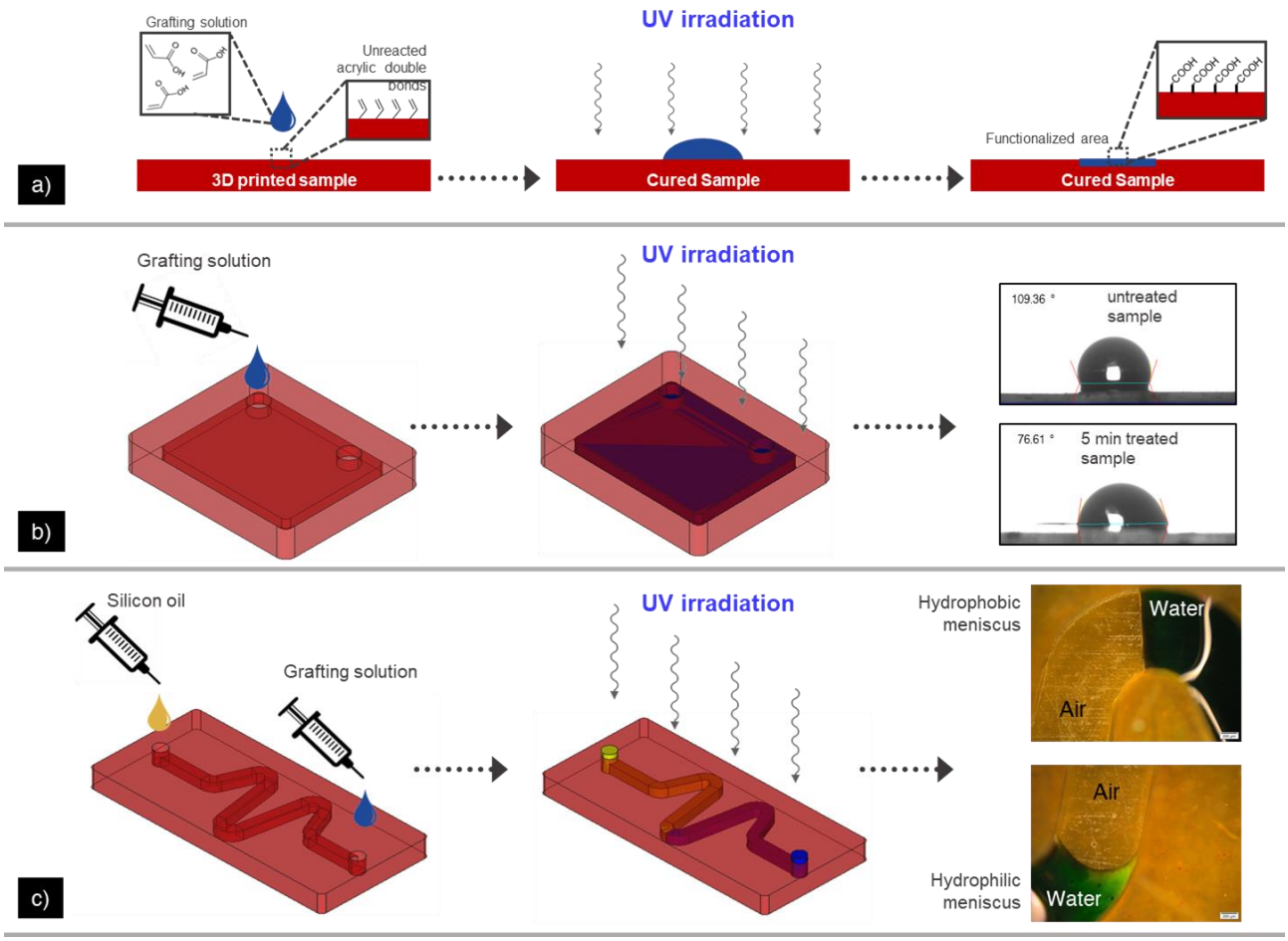

Figure 3. a) Sketch of surface modification by UV-Induced grafting polymerization on 3D printed flat silicone-samples, b) Sketch of surface modification chip with inner chamber and contact angel measurements for water droplets on unfunctionalized and functionalized surfaces; c) Sketch of surface modification for S-shaped microfluidic. The test shows the selective functionalization of the channel with the formation of a hydrophobic and hydrophilic meniscus inside the same channel.

The changes in water contact angle were measured for treated and untreated samples. The average contact angle of five samples for each experimental condition is shown in Figure 4.a. The wettability of the samples changes according to the UV-induced surface modification treatment: untreated TRAD samples presented a contact angle of 115.1° ± 0.5°, which drastically decreased to 58.9° ± 2.7° after 1 min of irradiation and did not further decrease for longer irradiation time. To confirm the presence of poly (acrylic acid), ATR-FTIR spectra were recorded on treated and untreated samples and the results are shown in Figure 4.b. The spectra were normalized using the 790 cm^{-1} peak corresponding to the Si-C asymmetrical bending or rocking vibration [66] (see Figure SI 9). The spectra reveal the presence of carboxylic acid groups with wide-ranging absorption bands of the O-H stretch around

3500-2500 cm^{-1},[67] as well as a sharp carbonyl peak (C=O) in the 1760-1690 cm^{-1} region. [68] All these results confirm the grafting of poly (acrylic acid) on the surface of silicone samples due to UV-induced grafting. As control experiment, we performed the same UV-induced surface functionalization treatment on 3D printed samples after post-curing step. Contac angle measurement (Figure SI10) shows that the surface remains strongly hydrophobic, indicating that the surface was not functionalized with poly(acrylic acid). It is thus crucial to perform the functionalization step during post-curing step in order to exploit efficently the unreacted acrylic double bonds.

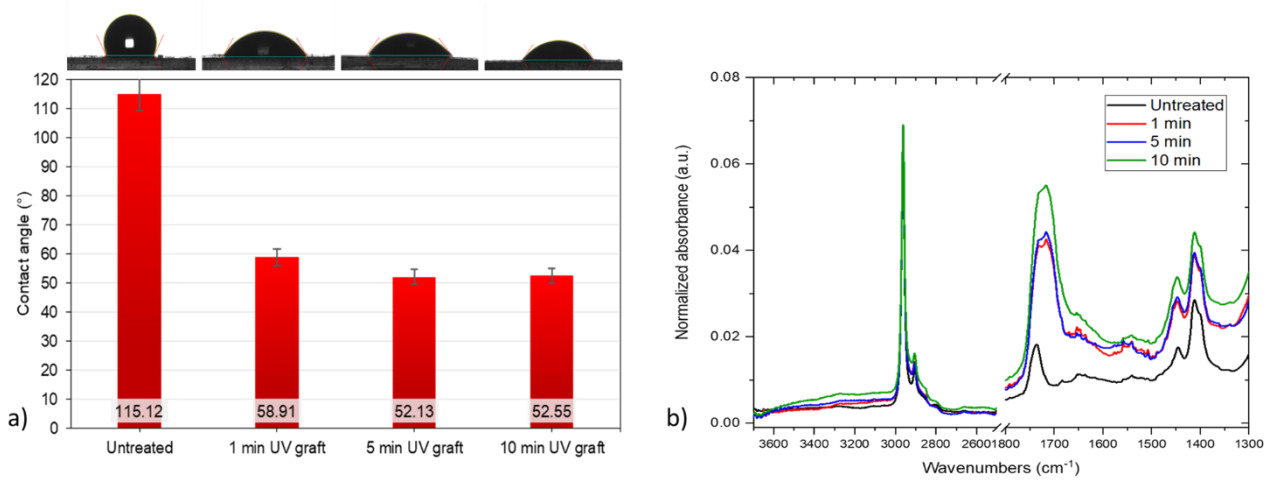

Figure 4. a) contact angle measurement and b) ATR-FTIR absorption spectra of TRAD samples after 1,5 and 10 minutes of UV-induced grating surface modification.

The next step investigated was to induce surface modification within the cavity of a 3D printed structure. For this purpose, chips with an inner chamber were designed and 3D printed as represented in Figure 3.b (see Figure SI 11.a for more details). The internal chamber (16x13x1 mm^3) was closed with a 1 mm thick cap-layer. A few drops of the AA-based grafting solution were introduced in the chamber, and then the samples were subjected to UV irradiation for 5 minutes. After the rising/washing protocol in ethanol and water, respectively, the top of the samples was cut lengthwise and changes in the wettability of the internal surfaces of the samples were determined. As shown in Figure 3.b, the water contact angle decreased from 109.36° to 76.61° for untreated and treated samples respectively. This confirms that the UV-induced surface modification can be performed even in a

closed 3D printed object, which in turn confirms the high light transparency at these wavelengths achieved by this technology for microfluid device preparation. A similar procedure was repeated on a 3D printed chip fabricated with one S-shaped channel with a cross-section of 1x1 mm^2. In this case, to selectively functionalize the surface of the channels (Figure SI 11.b for more details), we filled half of the microfluidic chip with silicon oil and the other half with the grafting solution (Figure 3.c). After 5 minutes of UV irradiation followed by the washing protocol, the inner surface wettability was analyzed by loading the channels with green colored deionized water and observing the changes in the stationary meniscus through optical microscopy Figure 3.c. As expected, a clear difference was observed between the two halves of the channel, passing from a hydrophobic meniscus in the unfunctionalized part of the channel to a hydrophilic meniscus in the UV-grafted side.

3. Conclusions

In this study we 3D printed acrylate-polydimethylsiloxane (PDMS) resins, processed through a commercial 3D-DLP printer: the final aim was to fabricate complex-shaped 3D printed microfluidic devices with engineered surfaces, to give robust alternatives to conventional PDMS technologies. At first, we performed a study on the photocurable formulation, properly selecting photoinitiator and dye to be compatible with the silicone resins. Then, ATR-FTIR and photorheology analyses were performed to study the photopolymerization progress and conversion and to obtain preliminary indications for the parameter optimization for the 3D printing step. Once the 3D printing settings were optimized, we fabricated complex-shaped 3D printed structures with truly three-dimensional channels. The 3D printed PDMS-based samples presented high chemical stability to different solvents and good mechanical properties, comparable to the conventional PDMS elastomer used for the fabrication of microfluidic devices, Sylgard 184. As a result of an appropriate choice of the materials for the preparation of the resin, the printed parts presented the required characteristics, such as flexibility, stretchability, and high optical transparency. These features are fundamental to produce microfluidic chips, demonstrating thus the compatibility of this application with DLP 3D printing.

Besides, the surface properties of 3D printed PDMS-based samples and chips were easily and selectively modified during the required post-curing procedure through UV-induced grafting polymerization. We demonstrated that even in closed 3D printed microfluidic it was possible to perform an easy surface functionalization taking advantage of the unreacted acrylic double bond remaining after the 3D printing step. This approach gives an added value in terms of surface properties to the printed devices as compared to classically produced microfluidics. The 3D printing of PDMS-based devices may potentially transform the conventional fabrication process for microfluidic devices by decreasing manufacturing costs and time, allowing the production of complex-shaped and truly three-dimensional microdevices.

4. Experimental

4.1 Materials

A silicone-based oligomer was used for the preparation of 3D printable formulations, TEGO®Rad 2800 (**TRAD**), which is an acrylate polydimethylsiloxane copolymer kindly supplied by Evonik Industries AG (Essen, Germany). The photoinitiator selected was a silicone-soluble derivate of phenyl bis(2,4,6-trimethylbenzoyl) phosphine oxide (**BAPO**) that for simplicity will be named **BAPO-Si**. BAPO-Si is a liquid BAPO photoinitiator developed by BASF and ETH Zurich for commercial use. It is a blend of a BAPO-methyl ester, a BAPO-isooctyl ester, and isooctanol obtained in an industrially feasible process (structures are shown in Figure SI 1.b). [49] Disperse red 1 methacrylate (**DR1-MA**), purchased from Merck, was used as a visible light absorber dye. Methyl methacrylate (**MMA**) monomer from Merck was used for solvating the dye. The chemical structures of the components for the resin preparation are shown in Figure SI 1. The other chemical solvents and reagents used for the different tests were purchased from Merck and used as received. Acetonitrile, Acrylic Acid (**AA**) and BAPO (all from Merck) were used for the functionalization step.

4.2 Preparation and 3D printing of formulations

For the preparation of the photocurable formulation, first 0.6 wt.% of the BAPO-Si photoinitiator was added to the TRAD oligomer and stirred at room temperature for six hours until the formulation became visibly homogeneous. Then the DR1-MA dye was dissolved in MMA (100 mg mL^{-1}), and a few drops of this solution were added to the TRAD formulation to obtain a concentration of 0.1 wt.% of DR1-MA. Finally, the formulation was kept under vacuum for 10 min at room temperature to degas.

The 3D printing of the resin was performed using an Asiga PICO 2 DLP-3D printer (Asiga, Australia). This 3D printer has a LED light source (405 nm), the nominal XY pixel resolution is 50 μm, the minimum Z-axis control is 1 μm. After preliminary studies and printing optimization, the best parameters were set to layer thickness 50 μm, light intensity 20 mW cm^{-2}, exposure time 10 seconds per layer. After the printing process, the structures were cleaned with compressed air and soaked in ethanol for 15 min at room temperature to remove the unreacted resin. UV post-curing processes were performed on the printed samples using a mercury arc lamp Dymax ECE device in the air (5 minutes, light intensity 10 mW cm^{-2}).

4.3 Sample Characterization

Photorheology: Real-time photorheological measurements were performed using an Anton Paar rheometer (Physica MCR 302); a Hamamatsu LC8 lamp with light emission in the visible range (wavelength > 400 nm) was used for the simultaneous irradiation during the tests. This lamp is equipped with an 8 mm light guide (light intensity on the sample surface 20 mW cm^{-2}). The measurements were performed in parallel-plate mode and the gap between the two plates was set to 0.1 mm. The experiments were performed at a constant temperature (25 °C), under a constant shear frequency (10 Hz) and at a strain amplitude of 0.1%. The irradiating light was turned on 1 minute after the beginning of the rheological measurement to stabilize the system before the onset of the

photopolymerization process. The changes in the viscoelastic moduli of the material during the polymerization process were measured as a function of exposure time.

ATR-FTIR spectroscopy: A Nicolet iS50 FT-IR spectrometer (Thermo Scientific, Milano, IT) equipped with attenuated total reflectance (ATR) accessory (Smart iTX) was used to investigate the acrylate conversion both of the liquid formulations and the 3D printed parts. The spectra were collected using an ATR accessory, collecting first the spectrum of the liquid TRAD formulation and then collecting the ATR spectra of the polymerized formulation after direct irradiation (with visible and UV light) on the ATR accessory. The formulation was irradiated using a visible portable lamp (Hamamatsu LC8 lamp, see description above) with a light intensity of 20 mW cm^{-2}, then the UV post-curing treatment was simulated by irradiating with UV portable lamp (Hamamatsu medium-pressure mercury lamp, a light intensity of 10 mW cm^{-2}). Spectra of 3D printed samples as printed and after different UV post-curing treatments were also collected. For the FTIR experiments, the spectra were collected with a resolution of 2 cm^{-1}, averaging 32 scans for each spectrum, wavenumbers range 650−4000 cm^{-1}. The conversion of acrylate double bonds was monitored by following the decrease of the peak area of the single carbon-oxygen bond of acrylates moieties, at 1196 cm^{-1}, whose vibration is modified by the opening of acrylate double bonds after photopolymerization. [52] The area of the acrylate peak was normalized by a constant signal in the spectra centered at 1257 cm^{-1} corresponding to methyl siloxane stretching vibrations. [53]

Extraction of unreacted residual resin procedure. To determine the extent of dissolution of polymerized samples toward various solvents, 3D printed TRAD samples (5mm x 5mm x 2mm, *lwh* = length x width x height) were immersed into ~2 mL of a solvent, using a metal net, for 24 hours at room temperature, then they were taken out from the vial and left dried overnight at 120 °C. The extraction percentage (wt.%) was determined by the mass difference of the sample before and after solvent extraction. For each solvent, the test was repeated three times.

Swelling percentage procedure. The swelling percentage (wt. %) in various solvents was determined to measure the weight difference between the swollen polymer and the pristine one. The samples

(5mm x 5mm x 2mm, *lwh*) were immersed into ~2 mL of the considered solvent, for different timeslots (5, 10, 15, 30, 60 minutes and 24 hours) at 25 °C. For each solvent, the test was repeated three times for accuracy.

Ultraviolet-visible spectroscopy. UV−vis measurements were conducted using a double-beam Lambda 40 instrument (PerkinElmer Italia, Milano, Italy). The samples were scanned in the range of 200−600 nm at a scan rate of 480 nm min^{-1}. UV-vis spectrometry was also used to analyze the solvents used for the extraction tests. For these experiments, the sample was immersed in a vial containing the solvent selected; then, after a certain time, the sample was removed, and UV-Vis spectra of the solvent were recorded. The procedure was repeated using fresh solvent after every immersing test until no absorbance peak is observed in the spectra after UV-VIS analysis.

Contact Angle Measurements. Static contact angles of the samples were determined using an FTA 1000C goniometer, equipped with a video camera and an image analyzer. The tests were performed at room temperature, using the sessile drop technique. A 3 µL droplet of deionized water (72.1 mN m^{-1}) was placed onto the sample surface and the static angle was measured. The five measurements were collected for each tested sample.

UV-induced surface modification: the surface of 3D printed TRAD specimens (10mm x 15mm x 1.5mm, *lwh*) was modified by UV-induced "grafting to" polymerization using a solution containing acrylic acid diluted in acetonitrile (100 mg mL^{-1}) and 2 wt.% of BAPO photoinitiator respect to the amount of acrylic acid. Few drops of the grafting solution were spread onto the samples, then UV-irradiated for different times (1, 5 and 10 min) was performed, using a high-pressure mercury arc lamp Dymax ECE with a light intensity of 10 mW cm^{-2}. After the UV-grafting treatment, the samples were rinsed in ethanol for 10 min and then in water for 30 minutes, to remove unlinked acrylic acid from the surface.

Mechanical testing: Tensile tests were conducted using an Instron 3360 dynamometer equipped with a load cell of 500 N. For each typology of samples, 5 specimens with a gauge length of 20 mm were produced and tested. The crosshead speed was set to 5 mm min^{-1}.

Supporting Information

Supporting Information is available from the Wiley Online Library or from the author.

Acknowledgments

The present work was developed in the framework of DEFLeCT project funded by Regione Piemonte POR-FESR 2014–2020

Received: ((will be filled in by the editorial staff))

Revised: ((will be filled in by the editorial staff))

Published online: ((will be filled in by the editorial staff))

Reference

[1] P. J. Kitson, M. H. Rosnes, V. Sans, V. Dragone, L. Cronin, *Lab Chip* **2012**, *12*, 3267.

[2] G. M. Whitesides, *Nature* **2006**, *442*, 368.

[3] M. Lake, C. Arciso, K. Cowdrick, T. Storey, S. Zhang, J. Zartman, D. Hoelzle, *Protoc. Exch.* **2015**, 1.

[4] M. Mehling, S. Tay, *Curr. Opin. Biotechnol.* **2014**, *25*, 95.

[5] T. Fujii, *Microelectron. Eng.* **2002**, *61–62*, 907.

[6] B. M. Paegel, R. G. Blazej, R. A. Mathies, *Curr. Opin. Biotechnol.* **2003**, *14*, 42.

[7] J. Scott Mellors, K. Jorabchi, L. M. Smith, J. Michael Ramsey, *Anal. Chem.* **2010**, *82*, 967.

[8] S. K. Vashist, P. B. Luppa, L. Y. Yeo, A. Ozcan, J. H. T. Luong, *Trends Biotechnol.* **2015**, *33*,

692.

[9] F. B. Myers, L. P. Lee, *Lab Chip* **2008**, *8*, 2015.

[10] M. Fanous, J. Ozhikandathil, S. Badilescu, M. Packirisamy, *2015 Photonics North* **2015**, DOI 10.1109/PN.2015.7292461.

[11] Y. Temiz, R. D. Lovchik, G. V. Kaigala, E. Delamarche, *Microelectron. Eng.* **2015**, *132*, 156.

[12] K. Ren, J. Zhou, H. Wu, *Acc. Chem. Res.* **2013**, *46*, 2396.

[13] S. Halldorsson, E. Lucumi, R. Gómez-Sjöberg, R. M. T. Fleming, *Biosens. Bioelectron.* **2015**, *63*, 218.

[14] A. Mata, A. J. Fleischman, S. Roy, *Biomed. Microdevices* **2005**, *7*, 281.

[15] I. D. Johnston, D. K. McCluskey, C. K. L. Tan, M. C. Tracey, *J. Micromechanics Microengineering* **2014**, *24*, DOI 10.1088/0960-1317/24/3/035017.

[16] G. W. Bishop, in *Microfluid. Biol. Fundam. Appl.*, **2016**, pp. 1–252.

[17] M. J. Beauchamp, G. P. Nordin, A. T. Woolley, *Anal. Bioanal. Chem.* **2017**, *409*, 4311.

[18] N. P. Macdonald, J. M. Cabot, P. Smejkal, R. M. Guijt, B. Paull, M. C. Breadmore, *Anal. Chem.* **2017**, *89*, 3858.

[19] A. Chiadò, G. Palmara, A. Chiappone, C. Tanzanu, C. F. Pirri, I. Roppolo, F. Frascella, *Lab Chip* **2020**, *20*, 665.

[20] R. D. Sochol, E. Sweet, C. C. Glick, S. Y. Wu, C. Yang, M. Restaino, L. Lin, *Microelectron. Eng.* **2018**, *189*, 52.

[21] N. Bhattacharjee, A. Urrios, S. Kang, A. Folch, *Lab Chip* **2016**, *16*, 1720.

[22] S. H. Huang, P. Liu, A. Mokasdar, L. Hou, *Int. J. Adv. Manuf. Technol.* **2013**, *67*, 1191.

[23] S. Ford, M. Despeisse, *J. Clean. Prod.* **2016**, *137*, 1573.

[24] S. Waheed, J. M. Cabot, N. P. Macdonald, T. Lewis, R. M. Guijt, B. Paull, M. C. Breadmore, *Lab Chip* **2016**, *16*, 1993.

[25] M. Hegde, V. Meenakshisundaram, N. Chartrain, S. Sekhar, D. Tafti, C. B. Williams, T. E. Long, *Adv. Mater.* **2017**, *29*, 1.

[26] T. A. Campbell, O. S. Ivanova, *Nano Today* **2013**, *8*, 119.

[27] S. V. Murphy, A. Atala, *Nat. Biotechnol.* **2014**, *32*, 773.

[28] S. Bose, S. Vahabzadeh, A. Bandyopadhyay, *Mater. Today* **2013**, *16*, 496.

[29] K. B. Anderson, S. Y. Lockwood, R. S. Martin, D. M. Spence, *Anal. Chem.* **2013**, *85*, 5622.

[30] B. C. Gross, J. L. Erkal, S. Y. Lockwood, C. Chen, D. M. Spence, *Anal. Chem.* **2014**, *86*, 3240−3253.

[31] D. Kokkinis, M. Schaffner, A. R. Studart, *Nat. Commun.* **2015**, *6*, DOI 10.1038/ncomms9643.

[32] F. Li, N. P. Macdonald, R. M. Guijt, M. C. Breadmore, *Lab Chip* **2019**, *19*, 35.

[33] S. Stassi, E. Fantino, R. Calmo, A. Chiappone, M. Gillono, D. Scaiola, C. F. Pirri, C. Ricciardi, A. Chiadò, I. Roppolo, *ACS Appl. Mater. Interfaces* **2017**, *9*, 19193.

[34] F. Frascella, G. González, P. Bosch, A. Angelini, A. Chiappone, M. Sangermano, C. F. Pirri,

I. Roppolo, *ACS Appl. Mater. Interfaces* **2018**, *10*, 39319.

[35] M. Zarek, M. Layani, I. Cooperstein, E. Sachyani, D. Cohn, S. Magdassi, *Adv. Mater.* **2016**, *28*, 4449.

[36] Y. Zhang, H. Li, X. Yang, T. Zhang, K. Zhu, W. Si, Z. Liu, *Polym. Compos.* **2016**, DOI 10.1002/pc.24117.

[37] G. Gonzalez, A. Chiappone, I. Roppolo, E. Fantino, V. Bertana, F. Perrucci, L. Scaltrito, F. Pirri, M. Sangermano, *Polymer (Guildf).* **2016**, *109*, 246.

[38] E. Fantino, A. Chiappone, I. Roppolo, D. Manfredi, R. Bongiovanni, C. F. Pirri, F. Calignano, *Adv. Mater.* **2016**, *16*, 3712.

[39] G. Taormina, C. Sciancalpore, M. Messori, F. Bondioli, *AIP Conf. Proc.* **2018**, *1981*, DOI 10.1063/1.5045927.

[40] Z. Li, C. Wang, W. Qiu, R. Liu, *Photochem. Photobiol.* **2019**, 1219.

[41] J. M. Sirrine, A. Zlatanic, V. Meenakshisundaram, J. M. Messman, C. B. Williams, P. R. Dvornic, T. E. Long, *Macromol. Chem. Phys.* **2019**, *220*, 1.

[42] N. Bhattacharjee, C. Parra-Cabrera, Y. T. Kim, A. P. Kuo, A. Folch, *Adv. Mater.* **2018**, *30*, 1.

[43] P. Taylor, I. L. Singer, J. G. Kohl, M. Patterson, **n.d.**, 37.

[44] B. G. R. J. Artus, S. Jung, J. Zimmermann, H. Gautschi, K. Marquardt, S. Seeger, **2006**, 2758.

[45] F. Wang, Y. Chong, F. K. Wang, C. He, *J. Appl. Polym. Sci.* **2017**, *134*, 1.

[46] C. Credi, G. Griffini, M. Levi, S. Turri, *Small* **2018**, *14*, 1.

[47] J. S. Manzano, Z. B. Weinstein, A. D. Sadow, I. I. Slowing, *ACS Catal.* **2017**, *7*, 7567.

[48] T. Zhao, X. Li, R. Yu, Y. Zhang, X. Yang, X. Zhao, L. Wang, W. Huang, *Macromol. Chem. Phys.* **2018**, *219*, 1.

[49] A. F. Cunningham, K. Misteli, K. Dietliker, B. Grimm, *Liquid Bisacylphosphine Oxide Photoinitiator*, **2015**, WO2015 / 004566.

[50] I. Roppolo, A. Chiappone, A. Angelini, S. Stassi, F. Frascella, C. F. Pirri, C. Ricciardi, E. Descrovi, *Mater. Horizons* **2017**, *4*, 396.

[51] P. Panjan, V. Virtanen, A. M. Sesay, *Analyst* **2018**, *143*, 3926.

[52] F. Masson, C. Decker, S. Andre, X. Andrieu, *Prog. Org. Coatings* **2004**, *49*, 1.

[53] J. Palaganas, A. C. de Leon, J. Mangadlao, N. Palaganas, A. Mael, Y. J. Lee, H. Y. Lai, R. Advincula, *Macromol. Mater. Eng.* **2017**, *302*, 1.

[54] F. P. W. Melchels, J. Feijen, D. W. Grijpma, *Biomaterials* **2010**, *31*, 6121.

[55] Y. Liao, J. Song, E. Li, Y. Luo, Y. Shen, D. Chen, Y. Cheng, Z. Xu, K. Sugioka, K. Midorikawa, *Lab Chip* **2012**, *12*, 746.

[56] H. Zirath, M. Rothbauer, S. Spitz, B. Bachmann, C. Jordan, B. Müller, J. Ehgartner, E. Priglinger, S. Mühleder, H. Redl, W. Holnthoner, M. Harasek, T. Mayr, P. Ertl, *Front. Physiol.* **2018**, *9*, 1.

[57] J. N. Lee, C. Park, G. M. Whitesides, *Anal. Chem.* **2003**, *75*, 6544.

[58] C. Toro, A. Thibert, L. De Boni, A. E. Masunov, F. E. Hernández, *J. Phys. Chem. B* **2008**, *112*,

929.

[59] S. Hu, X. Ren, M. Bachman, C. E. Sims, G. P. Li, N. L. Allbritton, *Anal. Chem.* **2004**, *76*, 1865.

[60] M. Ebara, J. M. Hoffman, P. S. Stayton, A. S. Hoffman, *Radiat. Phys. Chem.* **2007**, *76*, 1409.

[61] S. Sugiura, J. ichi Edahiro, K. Sumaru, T. Kanamori, *Colloids Surfaces B Biointerfaces* **2008**, *63*, 301.

[62] Z. Zhang, X. Feng, F. Xu, X. Liu, B. F. Liu, *Electrophoresis* **2010**, *31*, 3129.

[63] J. Zhang, Y. Chen, M. A. Brook, **2013**, DOI 10.1021/la403425d.

[64] G. González, X. Fernández-Francos, À. Serra, M. Sangermano, X. Ramis, *Polym. Chem.* **2015**, DOI 10.1039/C5PY00906E.

[65] C. F. Carlborg, T. Haraldsson, K. Oberg, M. Malkoch, W. Van der Wijngaart, *Lab Chip* **2011**, *11*, 3136.

[66] D. Cai, A. Neyer, R. Kuckuk, H. M. Heise, *J. Mol. Struct.* **2010**, *976*, 274.

[67] M. H. Schneider, B. Kozlov, H. Willaime, Y. Tran, F. Rezgui, P. Tabeling, *14th Int. Conf. Miniaturized Syst. Chem. Life Sci.* **2010**, *82*, 1949.

[68] W. Lee, T. G. Lee, W.-G. Koh, *J. Ind. Eng. Chem* **2007**, *13*, 1195.